Pergamon

Int. J. Heat Mass Transfer. Vol. 37, No. 17, pp. 2601–2613, 1994
Copyright © 1994 Elsevier Science Ltd
Printed in Great Britain. All rights reserved
0017-9310/94 $7.00+0.00

0017-9310(94)E0099-G

Developing laminar flow and heat transfer in a rectangular duct with one-walled injection and suction

Y. C. CHENG and G. J. HWANG†

Department of Power Mechanical Engineering, National Tsing Hua University, Hsinchu, Taiwan 300, Republic of China

and

M. L. NG

Energy and Resources Laboratories, Industrial Technology Research Institute, Chutung, Taiwan 310, Republic of China

(*Received* 9 *September* 1993 *and in revised form* 30 *March* 1994)

Abstract—This paper presents a numerical investigation on the developing laminar flow and forced convection in the entrance region of a rectangular duct with one wall subjected to a constant heat flux and a uniform fluid injection or suction. Using the pressure deviation and vorticity–velocity method, the three-dimensional Navier–Stokes equations and energy equation are solved simultaneously. Typical velocity and temperature distributions along the flow direction are reported, and both the hydrodynamic and thermal entrance lengths are examined. The phenomenon of flow reversal in suction flow is illustrated by variations of the axial pressure gradient. Friction factors and Nusselt numbers are also described for various wall Reynolds numbers and aspect ratios. Finally, a comparison of this numerical study with the existing data is made.

INTRODUCTION

FLOW and heat transfer in a duct with wall fluid injection or suction has been studied extensively in the past. Most of investigations dealt mainly with uniform transpiration for porous tubes or symmetric transpiration for porous parallel plates, and a few studies reported the results of semiporous ducts. There are numerous engineering applications for semiporous ducts, e.g. the vapor flow through a metal screen for food processing [1], and the solar air collectors [2, 3] using transpired metal plates. Jorne [4] and Lessner and Newman [5] studied the mass transfer along a one-porous-wall vertical channel in electrochemical systems. For transpiration cooling of turbine rotor blades, Soong and Hwang [6] worked on the laminar mixed convection in a radially rotating semiporous channel. In fuel cell stacks [7, 8], both the gaseous reactant flows of cathode and anode along an exothermic porous electrode are subjected to wall heat flux with fluid injection or suction. Among different types of cell stacks, the gas flow in one-porous-wall rectangular ducts for phosphoric acid [9], polymer electrolyte membrane [10] and molten carbonate fuel cells [11] can be found.

For two-dimensional, steady, laminar fully developed flow of an incompressible fluid in a one-porous-wall channel with uniform injection or suction, Donoughe [12] showed that equations of motion could be reduced to a fourth-order nonlinear ordinary differential equation by a similarity transformation, and obtained a third-order perturbation solution for the cases of suction or injection, $-4 < Re_w < 4$. Eckert *et al.* [13] performed a numerical analysis by employing the Runge–Kutta method for a wider range of the wall Reynolds number, $-13 < Re_w < 20$. The non-existence of a solution for $Re_w < -13$ was observed due to flow reversal at the impermeable wall. White [14] selected the power-series method to obtain an exact solution for the whole range of Re_w except for $Re_w < -11$. The flow reversal was observed at $Re_w = -11$. Recently, Soong and Hwang [6] applied the similarity transformation to the conjugated momentum and energy equations for laminar mixed convection in a radially rotating semiporous channel with constant wall heat flux. The fully developed velocity and temperature profiles were obtained by using the fourth-order Runge–Kutta scheme. Flow reversal was also observed and discussed in their results.

In the entrance region, Massey [1] solved the energy equation with weak injection, $0 < Re_w < 4$, by using an integral method. Rhee and Edwards [2] introduced the assumption of boundary-layer flow and a concept

†Author to whom correspondence should be addressed.

NOMENCLATURE

A cross-sectional area, ab
a height of a rectangular duct
b width of a rectangular duct
D_h hydraulic diameter, $4A/S$
f friction factor, $2\bar{\tau}_w/(\rho\bar{U}^2)$
h heat transfer coefficient
k thermal conductivity
L_{hy}, l_{hy} hydrodynamic entrance length and dimensionless hydrodynamic entrance length, $l_{hy} = L_{hy}/(ReD_h)$
L_{th}, l_{th} thermal entrance length and dimensionless thermal entrance length, $l_{th} = L_{th}/(PeD_h)$
M, N number of grids in the y and z directions
Nu local Nusselt number, hD_h/k
P, p pressure and dimensionless pressure, $p = P/(\rho\bar{U}_0^2)$
P', p' pressure deviation and dimensionless pressure deviation, $p' = P'D_h^2/(\rho\nu^2)$
$\bar{P}, \bar{p}$ pressure and dimensionless pressure averaged over a cross section, $\bar{p} = \bar{P}/(\rho\bar{U}_0^2)$
Pe Peclet number, $PrRe$
Pr Prandtl number, ν/α
Re local Reynolds number, $\bar{U}D_h/\nu$
Re_w wall Reynolds number, V_wD_h/ν
Re_0 inlet Reynolds number, $\bar{U}_0D_h/\nu$
S perimeter, $2(a+b)$
T temperature
U, V, W velocity components in the X, Y and Z directions, respectively
u, v, w dimensionless velocity components in the x, y and z directions, respectively, U/U_0, VD_h/ν, and WD_h/ν
X, Y, Z rectangular coordinates
x, y, z dimensionless coordinates, $X/(Re_0D_h)$, Y/D_h, and Z/D_h.

Greek symbols
α thermal diffusivity, $k/(\rho c_p)$
γ aspect ratio, a/b
θ dimensionless temperature, $(T-T_0)/(qD_h/k)$
ν kinematic viscosity
ξ vorticity defined by equation (9)
ρ density
τ shear stress.

Subscripts
b bulk fluid condition
c point of complete mass extraction
fd value in the fully developed region
t value at the upper wall
w wall condition
o inlet condition.

Superscripts
$\bar{}$ average value
$^+$ definition for $x^+ = x/Pr$
* normalized value.

of stream function. Quasi-linear equations of momentum and an energy equation with isothermal boundary conditions were solved using a finite-difference method. In addition, Sorour and Hassab [3] used the perturbation solution of axial velocities and the method of superposition to solve the energy equation for a semiporous channel with a constant wall heat flux. The eigenvalues were calculated using an implicit finite-difference scheme. Later, Sorour *et al.* [15] reworked the same problem using a quasi-linear technique for solving both the momentum and energy equations with non-uniform wall transpiration. Again, flow reversal appeared for strong suction rates.

For a three-dimensional flow, Hwang *et al.* [7, 8] used the vorticity–velocity method to obtain the flow and temperature fields in a square duct with one wall subjected to uniform fluid injection or suction and constant heat flux. However, aspect ratios other than 1 for small one-porous-wall rectangular ducts are frequently used in fuel cell stacks as shown in Fig. 1. The present paper investigates both the flow and heat transfer characteristics in a developing region of rectangular ducts with aspect ratios of 0.2, 0.5, 2 and 5. The interesting phenomena of fully developed flow, complete mass extraction, flow reversal as well as the results of friction factors and Nusselt numbers are presented.

THEORETICAL ANALYSIS

Consider a steady laminar flow of an incompressible fluid with constant physical properties flowing through a horizontal rectangular duct. The physical configuration and coordinate system are shown in Fig. 1. At the inlet of this duct, both the axial velocity and temperature distributions of the fluid are uniform. The lower wall of the duct is porous with uniform injection or suction and subjected to a constant heat flux, while the other three walls are impermeable and adiabatic. This injection fluid is the same as that of the mainstream and has the same temperature of the heated porous wall. For the case of suction flow, the above conditions are fulfilled automatically. In addition, the external force, compression work and viscous dissipation are all neglected.

In the fuel cell system in Fig. 1, a uniform chemical

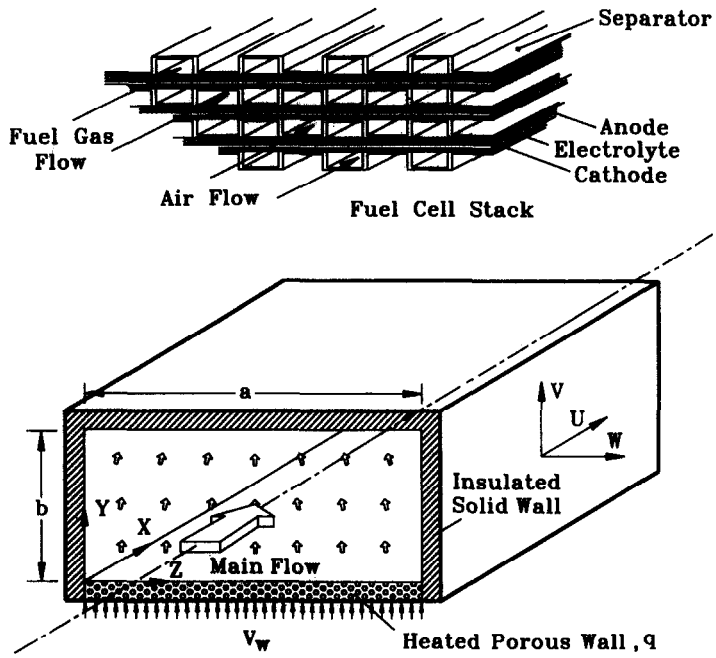

FIG. 1. Schematic diagram for fuel cell stack and coordinate system.

reaction rate is assumed in the plate between the anode and cathode; thus constant wall heat flux is used by many researchers [7–11]. In our laboratory, an experiment has been carried out for the thermal boundary condition by using an electric screen heater on the bottom duct wall. The injected air is heated separately to the wall temperature by a group of heaters before the air flows into the duct.

With the above assumptions, conservation equations for mass, momentum and energy can be listed as follows:

$$\nabla\cdot\mathbf{V}=0$$

$$(\mathbf{V}\cdot\nabla)\mathbf{V}=-\frac{1}{\rho}\nabla\bar{P}-\frac{1}{\rho}\nabla P'+\nu\nabla^2\mathbf{V}$$

$$(\mathbf{V}\cdot\nabla)T=\alpha\nabla^2T \qquad (1)$$

where $\bar{P}(X)$ is the averaged pressure over a cross section at axial location X, and $P'(X, Y, Z)$ is the pressure deviation induced by the entrance effect and fluid injection or suction. Referring to the coordinate system in Fig. 1, the following dimensionless variables and parameters can be introduced:

$$x=X/(D_hRe_0)\quad y=Y/D_h\quad z=Z/D_h$$
$$u=U/U_0\quad v=VD_h/\nu\quad w=WD_h/\nu$$
$$\bar{p}=\bar{P}/(\rho U_0^2)\quad p'=P'D_h^2/(\rho\nu^2)$$
$$\theta=(T-T_0)/(qD_h/k)\quad Re_0=U_0D_h/\nu$$
$$Re_w=V_wD_h/\nu\quad Pr=\nu/\alpha. \qquad (2)$$

At high inlet Reynolds number, $Re_0\gg1$, and high Peclet number, $Pe_0\gg1$, all axial diffusion terms in the momentum equations and the axial conduction term in the energy equation can be neglected. Hence the governing equations can be obtained in dimensionless forms as:

$$\frac{\partial u}{\partial x}+\frac{\partial v}{\partial y}+\frac{\partial w}{\partial z}=0 \qquad (3)$$

$$u\frac{\partial u}{\partial x}+v\frac{\partial u}{\partial y}+w\frac{\partial u}{\partial z}=-\frac{d\bar{p}}{dx}+\frac{\partial^2u}{\partial y^2}+\frac{\partial^2u}{\partial z^2} \qquad (4)$$

$$u\frac{\partial v}{\partial x}+v\frac{\partial v}{\partial y}+w\frac{\partial v}{\partial z}=-\frac{\partial p'}{\partial y}+\frac{\partial^2v}{\partial y^2}+\frac{\partial^2v}{\partial z^2} \qquad (5)$$

$$u\frac{\partial w}{\partial x}+v\frac{\partial w}{\partial y}+w\frac{\partial w}{\partial z}=-\frac{\partial p'}{\partial z}+\frac{\partial^2w}{\partial y^2}+\frac{\partial^2w}{\partial z^2} \qquad (6)$$

$$u\frac{\partial\theta}{\partial x}+v\frac{\partial\theta}{\partial y}+w\frac{\partial\theta}{\partial z}=\frac{1}{Pr}\left(\frac{\partial^2\theta}{\partial y^2}+\frac{\partial^2\theta}{\partial z^2}\right). \qquad (7)$$

The term, $\partial p'/\partial x$, in equation (4) is already eliminated under the assumption of high entrance Reynolds number. The initial and boundary conditions are

$$u-1=v=w=\theta=0 \quad \text{at entrance, } x=0$$

$$u=v-Re_w=w=\partial\theta/\partial y+1=0$$
$$\text{at porous wall, } y=0$$

$$u=v=w=\partial\theta/\partial y=0$$
$$\text{at impermeable wall, } y=\frac{1+\gamma}{2}$$

$$u=v=w=\partial\theta/\partial z=0$$
$$\text{at impermeable walls, } z=0 \text{ and } \frac{1+\gamma}{2\gamma} \qquad (8)$$

where γ is the aspect ratio of the rectangular duct. Referring to the coordinate system shown in Fig. 1, the value of Re_w is positive for injection flow, negative for suction flow and zero for impermeable flow. The solution of these equations depends on three independent parameters: the aspect ratio γ, the wall Reynolds number Re_w and the Prandtl number Pr.

In common practice, the magnitude of Re_w is smaller than 1 in fuel cells [9] and electrochemical cells [4, 5]. In addition, Re_w is between 1 and 10 for drying processes [1] and solar air collectors [2, 3]. For the purpose of engineering applications, $-20 < Re_w < 20$ is selected in the present investigation. Therefore, $Re_w \ll Re_0$ is assumed in this study for fast duct flow ($Re_0 \gg 1$).

To simplify further the governing equations, a vorticity function in the axial direction is defined as

$$\zeta = \frac{\partial w}{\partial y} - \frac{\partial y}{\partial z}. \tag{9}$$

By differentiating equation (9) and combining with continuity equation (3), the following equations for v and w can be derived:

$$\frac{\partial^2 v}{\partial y^2} + \frac{\partial^2 v}{\partial z^2} = -\frac{\partial \zeta}{\partial z} - \frac{\partial^2 u}{\partial y \partial x} \tag{10}$$

$$\frac{\partial^2 w}{\partial y^2} + \frac{\partial^2 w}{\partial z^2} = \frac{\partial \zeta}{\partial y} - \frac{\partial^2 u}{\partial z \partial x}. \tag{11}$$

By using a cross differentiation of pressure terms in equations (5) and (6) and combining with equation (3), a single equation for the axial vorticity can now be obtained:

$$u\frac{\partial \zeta}{\partial x} + v\frac{\partial \zeta}{\partial y} + w\frac{\partial \zeta}{\partial z} + \zeta\frac{\partial v}{\partial y} + \frac{\xi \partial w}{\partial z} + \frac{\partial u}{\partial y}\frac{\partial w}{\partial x} - \frac{\partial u}{\partial z}\frac{\partial v}{\partial x} = \frac{\partial^2 \zeta}{\partial y^2} + \frac{\partial^2 \zeta}{\partial z^2}. \tag{12}$$

Then equations (4), (10), (11), (12) and (7) for u, v, w, ζ, and θ can be solved. The pressure gradient, $-\mathrm{d}\bar{p}/\mathrm{d}x$, in equation (4) is determined by the overall mass balance,

$$\bar{u} = 1 + \frac{2}{1+\gamma} Re_w x \tag{13}$$

where $\bar{u}$ is the averaged axial velocity obtained from the solution of equation (4).

The local friction factor can be computed by using the wall velocity gradients,

$$f Re = \frac{2\gamma}{(1+\gamma)^2}\frac{1}{\bar{u}}\left(\int \left.\frac{\partial u}{\partial y}\right|_{y=0} \mathrm{d}z - \int \left.\frac{\partial u}{\partial y}\right|_{y=(1+\gamma)/2} \mathrm{d}z + 2\int \left.\frac{\partial u}{\partial z}\right|_{z=0} \mathrm{d}y\right) \tag{14}$$

and the local Nusselt number can also be calculated from an average temperature difference between the heated wall and the bulk mean fluid,

$$Nu = \frac{1}{\bar{\theta}_w - \bar{\theta}_b} \tag{15}$$

where θ_b is the bulk mean temperature difference defined as

$$\theta_b = \frac{4\gamma}{(1+\gamma)^2}\frac{1}{\bar{u}}\int\int u\theta \,\mathrm{d}y \,\mathrm{d}z. \tag{16}$$

METHOD OF SOLUTION

To find a solution analytically for the unknowns, u, v, w, ζ and θ in this problem is beyond contemplation. Hence, a numerical finite-difference scheme based on the vorticity–velocity method [16] is employed to obtain the simultaneous solutions at each desired axial location with different γ and Re_w. The three parabolic–elliptic partial differential equations (4, 12, 7) for u, ζ and θ are solved by the Du Fort–Frankel matching scheme, and the other two elliptic equations (10, 11) are solved by the alternating direction implicit scheme. The average axial pressure term, $-\mathrm{d}\bar{p}/\mathrm{d}x$, is adjusted iteratively to meet the constraint of overall mass balance at each axial location. It usually takes only three steps to get an accurate value for this axial pressure gradient. The detailed numerical procedures can be found in Hwang *et al.* [7].

For a better numerical accuracy, different cross-sectional meshes were used for different aspect ratios. Numerical experiments were carried out to ensure the accuracy of the results on the step and mesh sizes, even at strong injection and suction conditions which may cause stiff velocity and temperature gradients. Table 1 presents the results of numerical experiments. For the cases listed in this table, most of the variations in the friction factors, $f Re$, and Nusselt numbers, Nu, are less than 1% at all axial positions. Although the differences of Nu for the cases $\gamma = 0.2$, 0.5 and 1.0 are slightly higher at $x = 0.001$ for injection flow $Re_w = 20$, the values are still less than 2%.

As a partial verification of the computation, the hydrodynamically developing flow was calculated without mass transpiration. These results are compared with Curr *et al.* [17], and the differences in friction factors are within 1% at all axial locations for $\gamma = 1.0$. Due to the lack of simultaneously developing flow data for rectangular ducts with one heated wall in the available literature, only the fully developed friction factors and Nusselt numbers for various aspect ratios are compared as shown in Table 2. The peripherally averaged friction factors deviate within 1.0% from those of Shah and London [18], and the averaged Nusselt numbers deviate within 1.7% from those of Schmidt and Newell [19] except for the case of $\gamma = 0.2$ which is 4.3% because of the coarse 10×10 finite-difference grids used. All the present calculations were performed on an IBM 560 workstation. Typical computation time is approximately 60–90 CPU minutes for computation down to the axial distance $x = 0.1$. It is noted that the computation time

Table 1. Numerical experiments for grids and step sizes ($Pr = 0.72$)

Re_x	Aspect ratio		0.2		0.5		1.0		2.0		5.0	
x	Grid. No., $M \times N$		31×81†	41×91	41×61†	51×71	51×51†	61×61	61×41†	71×51	81×31†	91×41
	Step size $\times 10^5$		5.0	2.5	5.0	2.5	5.0	2.5	5.0	2.5	5.0	2.5
x/Re_x	$p_w = 20$											
$= 0.001$		$f\,Re$	32.64	32.60	31.52	31.68	31.62	31.83	32.75	32.93	35.02	35.01
		Nu	8.358	8.508	7.957	8.094	7.531	7.645	7.169	7.224	6.860	6.853
x/Re_x	$= 0.01$	$f\,Re$	24.17	24.23	22.27	22.33	21.38	21.44	21.44	21.48	22.48	22.50
		Nu	2.040	2.039	1.695	1.690	1.384	1.378	1.108	1.102	0.857	0.850
x	$= 0.1$	$f\,Re$	24.12	24.17	21.94	21.98	20.72	20.83	20.24	20.28	21.06	21.11
		Nu	0.920	0.921	0.632	0.630	0.407	0.405	0.241	0.240	0.127	0.126
x/Re_x	$p_w = -20$‡											
$= 0.001$		$f\,Re$	42.57	42.79	39.20	39.53	37.10	37.48	36.11	36.43	36.48	36.56
		Nu	23.53	23.66	23.17	23.34	22.86	23.04	22.57	22.75	22.67	22.73
x/Re_x	$= 0.01$	$f\,Re$	30.66	31.09	25.38	25.61	22.36	22.51	21.28	21.39	21.96	22.04
		Nu	16.62	16.50	16.12	16.08	15.81	15.78	15.71	15.66	16.11	15.97
	$= 0.1$	$f\,Re$	—	—	—	—	—	—	—	—	20.77	20.85
		Nu	—	—	—	—	—	—	—	—	15.20	15.07

†The number of grids and step sizes used in the present study.

‡Flow reversal at $x = 0.011$ for $\gamma = 0.2$, $x = 0.0156$ for $\gamma = 0.5$, and $x = 0.0294$ for $\gamma = 1.0$, and complete mass extraction at $x = 0.075$ for $\gamma = 2.0$ and $x = 0.225$ for $\gamma = 5.0$.

Table 2. Comparison of fully developed friction factors and Nusselt numbers of impermeable duct flow

γ	$f Re$	$f Re$†	Nu	Nu‡
0	23.95§	24.00	5.374§	5.385
0.2	19.01	19.07	4.223(31 × 81)	4.411
0.5	15.50	15.55	3.489(41 × 61)	3.539
1.0	14.19	14.23	2.681(51 × 51)	2.712
2.0	15.50	15.55	1.830(61 × 41)	1.854
5.0	19.01	19.07	0.948(81 × 31)	0.964

† Shah and London [18].
‡ Schmidt and Newell [19], grid size 10 × 10.
§ The values were obtained for $\gamma = 0.001$.

depends mainly on the length of axial distance, the aspect ratio and the magnitude of injection or suction velocity through the porous wall.

RESULTS AND DISCUSSION

For exploring the flow and heat transfer characteristics, the effects of fluid injection or suction and the aspect ratio on the development of axial velocity and temperature profiles in the rectangular duct are discussed. Both the hydrodynamic and thermal entrance lengths are examined for a further understanding of the problem. The interesting phenomena of fully developed flow, complete mass extraction and flow reversal are illustrated. The friction factors and Nusselt numbers in the entrance as well as the fully developed regions are described for various wall Reynolds numbers and aspect ratios. Finally, a comparison of this numerical study with existing data is included.

Velocity development

The axial velocity profiles along the rectangular duct with injection for different wall Reynolds numbers are presented in Figs. 2(a) and 2(c) for $\gamma = 0.5$ and 2.0, respectively. The dimensionless velocities shown by solid lines are on the center plane perpendicular to the porous wall. The fluid injection induces both mass addition and blowing force from the porous wall; thus it increases the axial velocity and shifts its peak away from the porous wall. Due to more fluid injection, for larger Re_w, larger x or smaller γ, the increment of axial velocity is bigger, and the velocity shift is more pronounced. Figures 2(b) and 2(d) show the cases of suction flow. In contrast, fluid suction induces both mass subtraction and withdrawal force from the porous wall; thus it decreases the axial velocity and shifts its peak towards the porous wall. The velocity components shrink along the axial distance until the flow reaches the point of complete mass extraction or flow reversal. This shrinking of axial velocities and the shift of velocity peak are more pronounced with stronger suction, larger x or smaller γ.

The effect of aspect ratio on the axial velocity development is illustrated in Figs. 2(e) and 2(f) for $Re_w = 5$ and -5, respectively. It is known that the maximum axial velocity for the case of $\gamma = 1$ is the largest one among those for $\gamma \lessgtr 1$ with a fixed mass flow, but it is not true in a duct with either injection or suction. For injection flow, the mass additions for $\gamma = 0.2$ and $\gamma = 0.5$ are larger than for $\gamma = 1$; thus their axial velocities are larger than for $\gamma = 1$ along the axial distance. However, due to smaller mass additions, the velocity profiles for $\gamma = 2$ and 5 are flatter than that for $\gamma = 1$ as depicted in Fig. 2(e). In addition, the upward shifts of axial velocity peaks for $\gamma = 0.2$ and 0.5 are slightly lower than for $\gamma = 1$. As noted in Fig. 2(f) for suction flow, the effect of mass subtraction on u is more significant when γ is smaller, and the peaks of velocity profiles along the duct are higher when γ is larger. It is also shown by the dotted lines in Figs. 2(a)–2(f) that the normalized velocities, $u^* = U/\bar{U}$, are very similar to each other for different wall Reynolds numbers and also similar to those of constant mass flow for different aspect ratios.

In Fig. 3, the constant-velocity maps of u, v and w in the transverse cross sections for $\gamma = 0.5$ are plotted. All values of u, v and w on four walls are zero except $v = Re_w$ on the lower porous wall. The location marked with a positive or negative sign represents the point with the highest absolute value of velocity. The flow is in the hydrodynamically developed region for case (a), near the section of complete mass extraction for case (b), and in the region of flow reversal for case (c). Between these three cases, the flow patterns of v and w are similar; however, a significant difference is observed for u. The shifts of axial velocity peak are in opposite directions for injection and suction flow as shown in cases (a) and (b), and a pair of reverse flows occur on the upper corners of the cross section as shown in case (c).

Hydrodynamic entrance length, complete mass extraction and flow reversal

When the fluid with uniform inlet velocity distribution flows into the entrance of a one-porous-wall rectangular duct, the inertia force, friction force, injection or suction force and pressure force all interact with one another. The velocity, $U_{max}/\bar{U}$, will be constant in the fully developed region if a normalized

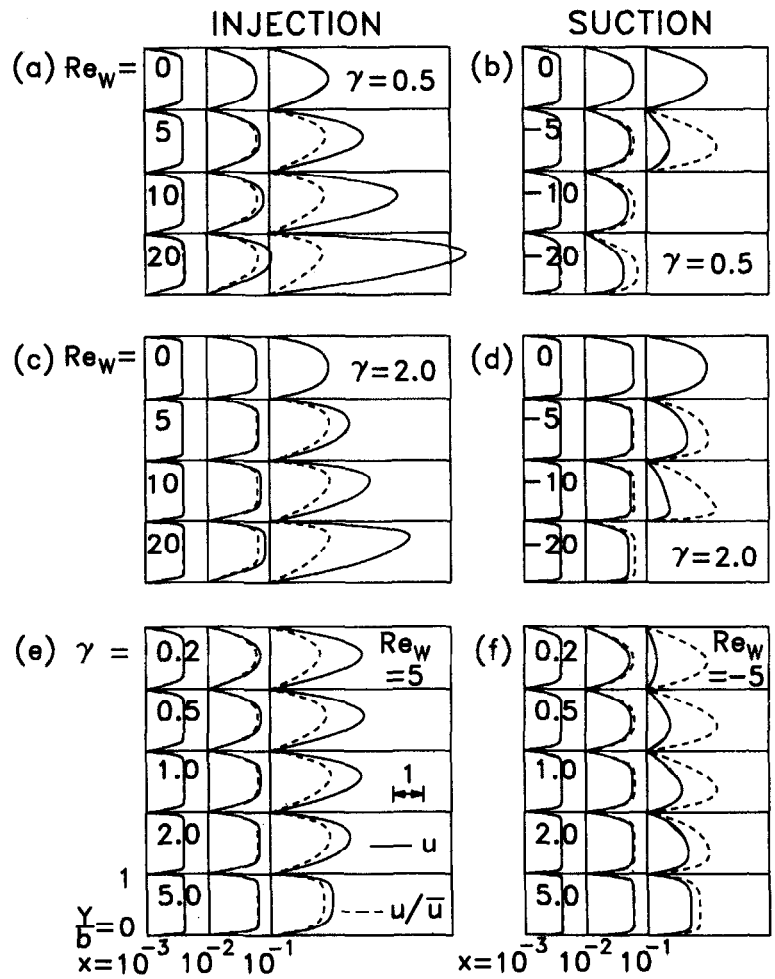

FIG. 2. Dimensionless axial and normalized velocity distributions at different axial positions.

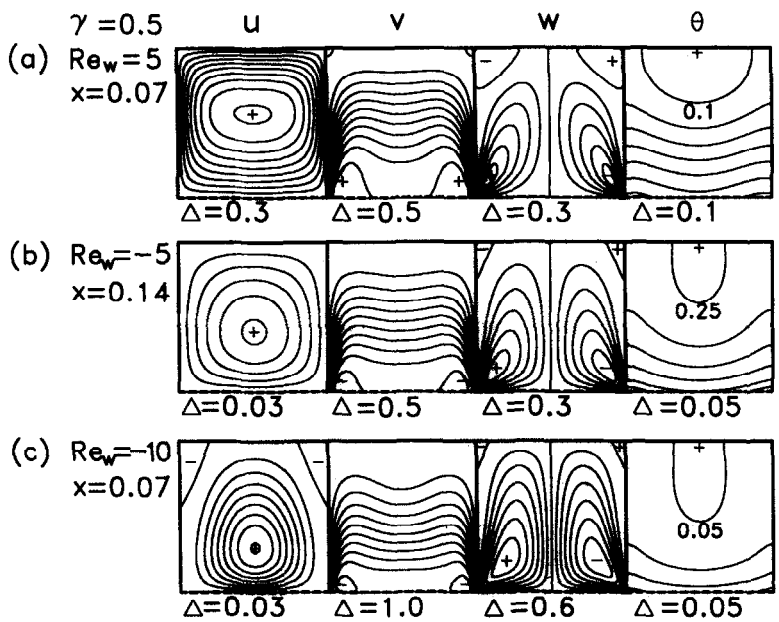

FIG. 3. Constant velocities and isotherm maps for $\gamma = 0.5$: (a) injection, $Re_w = 5$, $x = 0.07$, (b) suction, $Re_w = -5$, $x = 0.14$, (c) suction, $Re_w = -10$, $x = 0.07$.

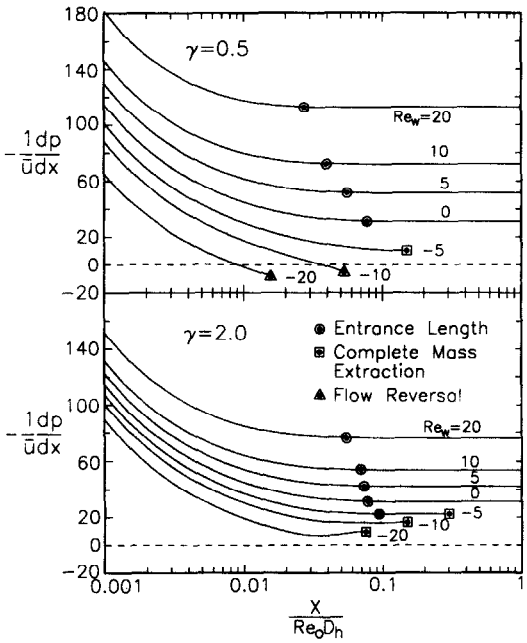

FIG. 4. Wall Reynolds number effects on normalized axial pressure gradients along the axial direction.

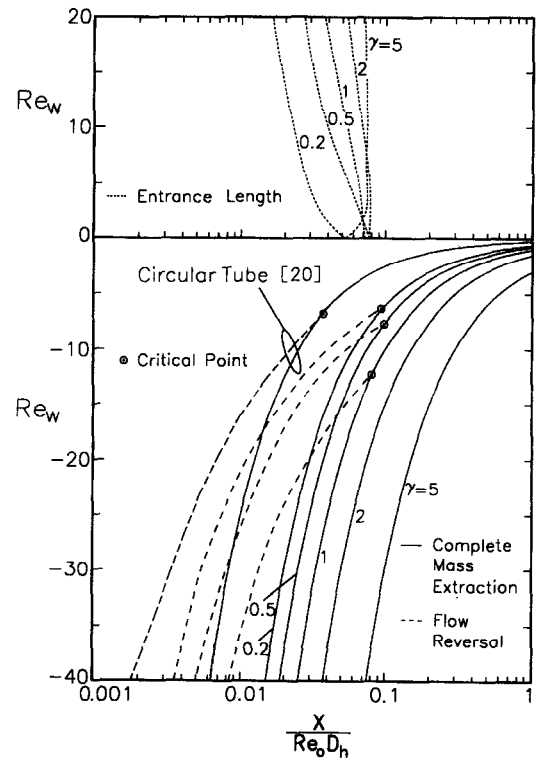

FIG. 5. Entrance lengths, locations of complete mass extraction and flow reversal under different aspect ratios and suction conditions.

axial pressure gradient is constant. As shown in Fig. 4, the pressure gradient cannot drop to a constant value for $\gamma = 0.5$ and $Re_w = -5, -10, -20$, as well as $\gamma = 2$ and $Re_w = -10, -20$; hence the flow cannot reach its fully developed region. The hydrodynamic entrance length, l_{hy}, is usually defined as the duct length required to achieve a maximum axial velocity of 99% of the corresponding fully developed value. Using this definition, the variations of entrance lengths for different Re_w and γ are shown in Fig. 5. In general, the hydrodynamic entrance length is decreased by fluid injection ($Re_w > 0$) for $\gamma \leqslant 2$, except for $\gamma = 5$. A duct with lower aspect ratio and stronger injection means a higher mass input to the channel, hence a shorter l_{hy} can be expected. In most of the cases for suction flow, the hydrodynamically fully developed region cannot be reached due to the complete mass extraction or flow reversal.

It is understandable that the point of complete mass extraction, x_c, in a suction flow along the rectangular duct can always be achievable. Using the mass balance, one has the value x_c:

$$x_c = \frac{1+\gamma}{2|Re_w|}. \tag{17}$$

The values of x_c are plotted with solid lines in Fig. 5 for various γ and Re_w, and the axial distances of flow reversal detected numerically are plotted by dashed lines. As pointed out by Quaile and Levy [20], the laminar flow in a porous tube may be changed to turbulence with a sufficiently large wall suction. Therefore, their results for complete mass extraction and flow reversal are also included in this figure. Due to the stronger outward suction force, flow reversal occurs earlier with larger suction rate and lower aspect ratio. However, flow reversal has never been observed numerically for $\gamma = 2$ and 5 for $Re_w = 0$ to -40. When the fluid is extracted slowly from the porous wall, its mass in a local cross section diminishes gradually along the axial direction and finally vanishes at the point of complete mass extraction. But, with a strong suction, the fluid in the cross section cannot fill the vacancies caused by the extraction and thus flow reversal is created locally at that specific axial position. Obviously, flow reversal occurs because no more axial momentum can be withdrawn ($u_w = 0$). Thus the decreasing axial momentum must be balanced by a pressure rise. This adverse pressure gradient reverses the flow where its velocity is small.

The normalized axial pressure gradients, $-(1/\bar{u})(d\bar{p}/dx)$, along the axial direction can be illustrated by using Fig. 4 with various wall Reynolds numbers for $\gamma = 0.5$ and 2. For the cases of $Re_w \geqslant 0$, this normalized quantity gradually decreases in the developing region, and an asymptotic value is attained in the fully developed region. The fully developed value is larger for higher Re_w to overcome the flow resistance induced by injection. In most cases of suction flows, the pressure gradient reduces continuously without an asymptotic value along the duct due to mass subtraction. However, the pressure gradient for $\gamma = 2$ and $Re_w = -5$ drops gradually to a fully developed constant value before the complete mass

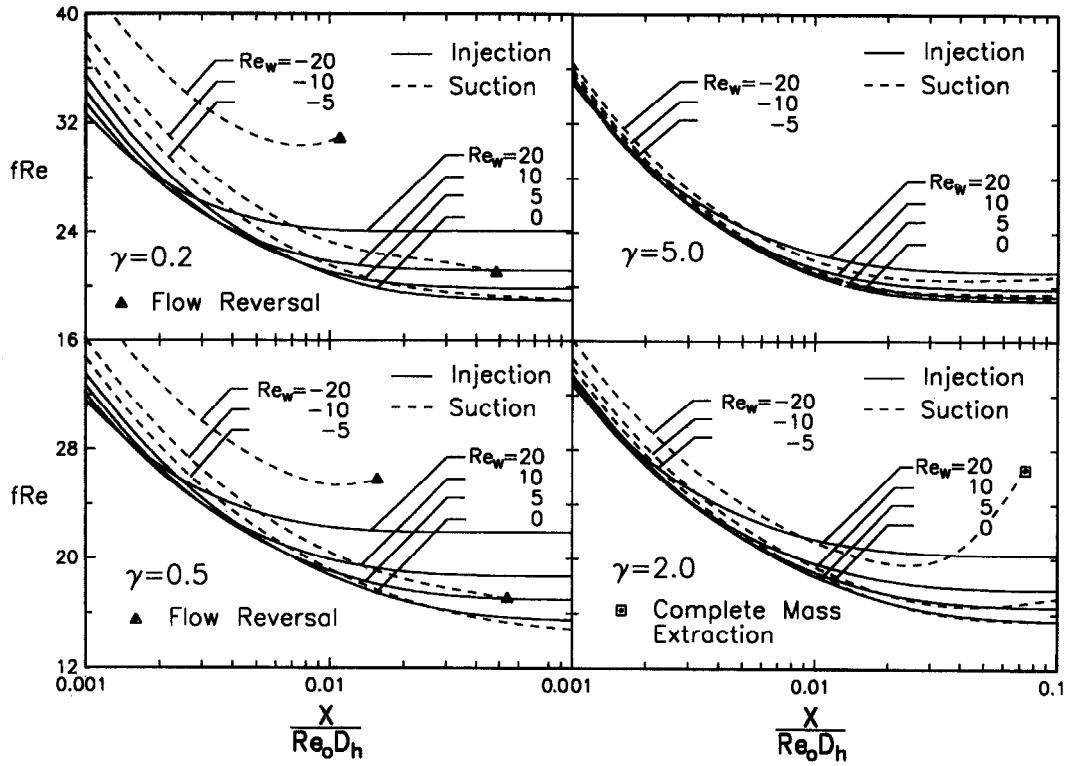

FIG. 6. Variations of friction factors along the axial direction for $\gamma = 0.2$, 0.5, 2.0 and 5.0 with various values of Re_w.

extraction. The curves drop to negative values for $\gamma = 0.5$ and $Re_w = -10$ and -20. As can be seen also in Fig. 5, flow reversal occurs at specific axial positions with these negative pressure gradients.

Developing and developed friction factors

The variations of skin friction, fRe, along the axial direction in a rectangular duct for both injection and suction flows with $\gamma = 0.2$, 0.5, 2.0 and 5.0 are shown in Fig. 6. For injection flow, the friction factor decreases with the increase in Re_w in the inlet region. In contrast, it increases with the increase in Re_w at $x > 0.003$. As indicated by equation (14), the local friction factor is affected by both the average axial velocity and the wall velocity gradient for a specific aspect ratio. In the inlet region, axial velocity gradients are almost the same for different Re_w, but the average axial velocity is larger for larger Re_w. As a result, friction factors are dominated by the average axial velocity. However, when the flow is further developed along the axial direction, the wall velocity gradient dominates the variation of friction factor. Consequently, increasing wall velocity gradients due to larger wall Reynolds numbers results in higher values of friction factors.

For suction flow, the friction factor increases with increasing rate of suction in the whole region as shown in Fig. 6. However, at large x, the variations in the friction factor become more complicated due to the effect of mass reduction. For the case of $\gamma = 2$, the values of fRe decrease and then increase after $x = 0.04$ and 0.025 for $Re_w = -10$ and -20, respectively. The existence of the inversion points is due to the effect of strong mass extraction. For the cases of $\gamma = 0.2$ and 0.5, fluid suction induces flow reversal at a specific point before the flow reaches the point of complete mass extraction for $Re_w = -10$ and -20, and all the fluid can be completely extracted without flow reversal for $Re_w = -5$. The friction factor decreases continuously for $Re_w = -5$ and -10 along the axial direction, but increases slightly after $x = 0.01$ for $Re_w = -20$.

The fully developed friction factors for injection flow with various aspect ratios are presented in Fig. 7. This figure does not include the cases of suction flow in which the hydrodynamically developed regions exist only for weak suction. As the aspect ratio is specified, the friction factor is always larger for a stronger injection flow due to a larger axial velocity gradient. In this figure, Shah and London's data [18] for impermeable flow in a rectangular duct are also included for comparison; the differences between these data and calculated results of this study are small.

Development of temperature profile

The effect of Re_w on dimensionless temperature profiles at axial distances $x^+ = 0.001$, 0.01, 0.1 and 1 for both injection and suction flows are shown in Fig. 8.

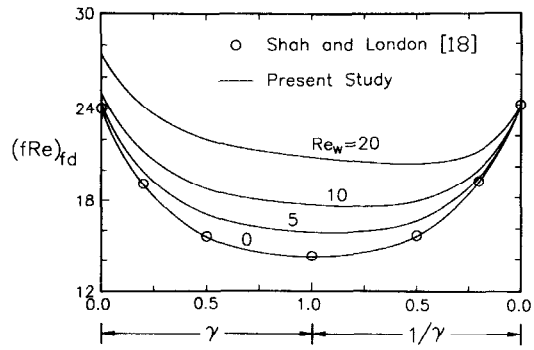

FIG. 7. Fully developed friction factors of various injection flows in the rectangular ducts.

These data are all on the center plane perpendicular to the porous wall. As a common practice, the coordinate, $x^+ = x/Pr$, is used in these figures. Because heat is transferred from the porous wall, the temperature in the lower part is always higher than that in the upper part, and the temperature of injection flow is always higher than that at the same position of the suction flow.

For injection flow, the temperature of the fluid in a rectangular duct arises by both wall heat flux and fluid injection. Since the upper wall is adiabatic and the center portion of the duct is cooled by upstream fluid, the increment of temperature is more pronounced for the fluid at the lower part of a cross section. For a specified aspect ratio, this increment is more significant due to a larger amount of heat input by the injected fluid for larger Re_w and x. As less fluid is injected for larger γ, the thermal resistance along the y direction is increased. This explains that the temperature difference along the y direction for larger γ is greater than that for small γ. It is also noted that the temperature is out of scale in Fig. 8(c) for $Re_w = 20$ and is not plotted here. For suction flow, the fluid temperature can arise by heat conduction from the porous wall. As part of the thermal energy is carried away by the extracted fluid, the fluid temperature

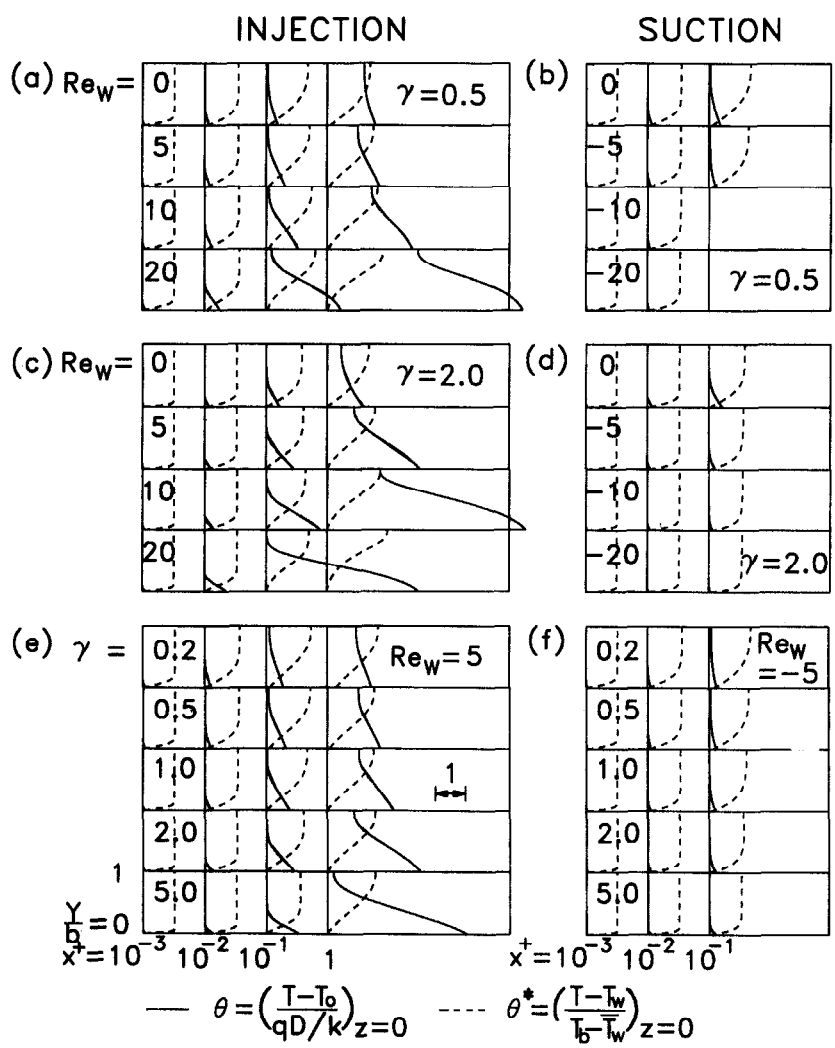

FIG. 8. Axial dimensionless and normalized temperature distributions at different axial distances.

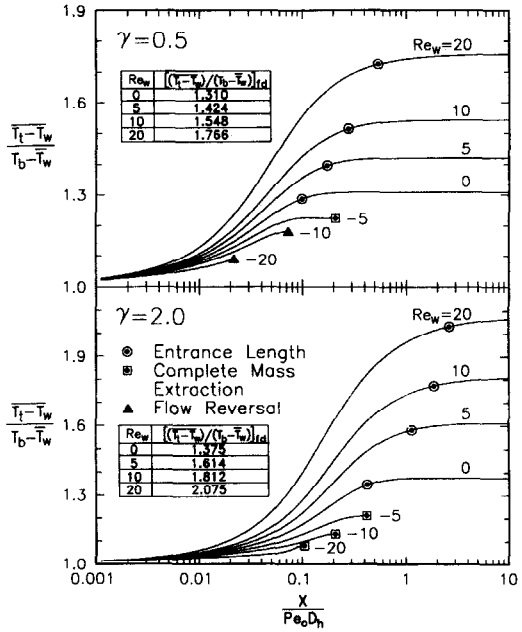

FIG. 9. Wall Reynolds number effects on normalized temperatures on the upper wall along the axial direction.

increases slowly along the axial distance, and temperature is higher for lower suction rate. Due to larger heat conduction area in a duct with smaller γ, the fluid temperature is higher.

The effect of aspect ratio on the temperature development is illustrated in Figs. 8(e) and 8(f) for $Re_w = 5$ and -5, respectively. Since the bottom porous wall is longer, more heat is conducted and more fluid is extracted for small γ; then the fluid temperature increases quickly for $\gamma = 0.2$, but slowly for $\gamma = 5$. It is also observed that, due to greater thermal resistance, the temperature of the porous wall is higher for larger aspect ratio in injection flow.

Thermal entrance length

To determine the characteristics of the thermal entrance length more closely, a normalized temperature θ^* defined. $\theta^* = (T-\bar{T}_w)/(T_b-\bar{T}_w)$ is used. The development of this normalized temperature profile is plotted by dashed lines in Fig. 8. For most cases, the temperature profiles are not only similar to each other but also invariant as the flow moves along the duct. Subsequently, the flow can be considered as thermally fully developed. However, the temperature similarity and invariance cannot be found for the cases of high aspect ratio and strong suction. In order to identify the variation of temperature along the axial distance, a specific local temperature has to be chosen. Because the heat is input from the bottom porous wall, the temperature of the upper wall is the slowest to rise and the least sensitive. The variations of average upper wall temperature, $\overline{\theta_t^*}$, along the duct for $\gamma = 0.5$ and 2 is shown in Fig. 9. It is clearly noted that the normalized fluid temperature increases to an asymptotic constant at a specific axial location for all injection cases, but cannot approach an asymptotic value for the cases of strong suction.

The dimensionless thermal entrance length can be expressed as $l_{th} = L_{th}/(PeD_h)$ and is plotted in Fig. 9. Its value is determined by observing $\overline{\theta_t^*}$ reaching an asymptotic value. The entrance length is longer for higher aspect ratio in impermeable flow, and the same result is also obtained in injection flow. Usually the thermally fully developed region cannot be achieved for suction flow, except for the weak suction case.

Developing and developed Nusselt numbers

The effect of Re_w on Nusselt numbers along the axial direction for $Pr = 0.72$ with $\gamma = 0.2$, 0.5, 2.0 and 5.0 is given in Fig. 10. As can be seen, the Nusselt number is reduced by fluid injection and is increased by fluid suction. This is similar to the solutions of Pederson and Kinney [21] for porous tubes as well as Doughty and Perkins [22] for porous parallel plates. According to equation (15), Nu is a reciprocal of $\overline{\theta_w - \theta_b}$, and this value for injection flow gradually approaches an asymptotic value in the fully developed region. In the case of suction flow, the temperature difference of heated wall and bulk fluid is reduced by fluid extraction, and hence the Nusselt number is larger than that of injection flow at the same axial position. The results show that a smaller aspect ratio induces higher values of Nusselt number for both cases of injection and suction flow. The reason is that the fluid mixes well in the duct with small γ, as can be seen in Figs. 8(e) and (f).

Fully developed Nusselt numbers for injection flow with various aspect ratios are presented in Fig. 11. This figure does not include the cases of suction flow, because the developed regions only exist for weak suction. For a fixed aspect ratio, the Nusselt number is always smaller with stronger injection. For large injection such as $Re_w = 20$, Nu is very small; hence the thermal energy input to the flow is mainly from the injected fluid. In this figure, Schmidt and Newell's data [19] for impermeable flow in a rectangular duct are also included for comparison; the differences between these data and calculated results of this study are small.

Comparison with existing data for case $\gamma \to 0$

Among limited data available in the literature, Doughty and Perkins' results [22, 23] can be selected for comparison with the present data. Their results are for hydrodynamically and simultaneously developing laminar flows between parallel porous plates subjected to constant heat flux. In the present numerical scheme, $\gamma = 0.001$ and symmetric porous walls are taken to obtain the comparable data. Figure 12(a) shows that the results of the friction factor are in good agreement with each other, even in the inlet region of the channel. Moreover, near the location of flow reversal caused by strong suction for $Re_w = -20$, the friction factors are also very close. In addition, the present Nusselt numbers for $\gamma = 0.001$ along the channel are plotted

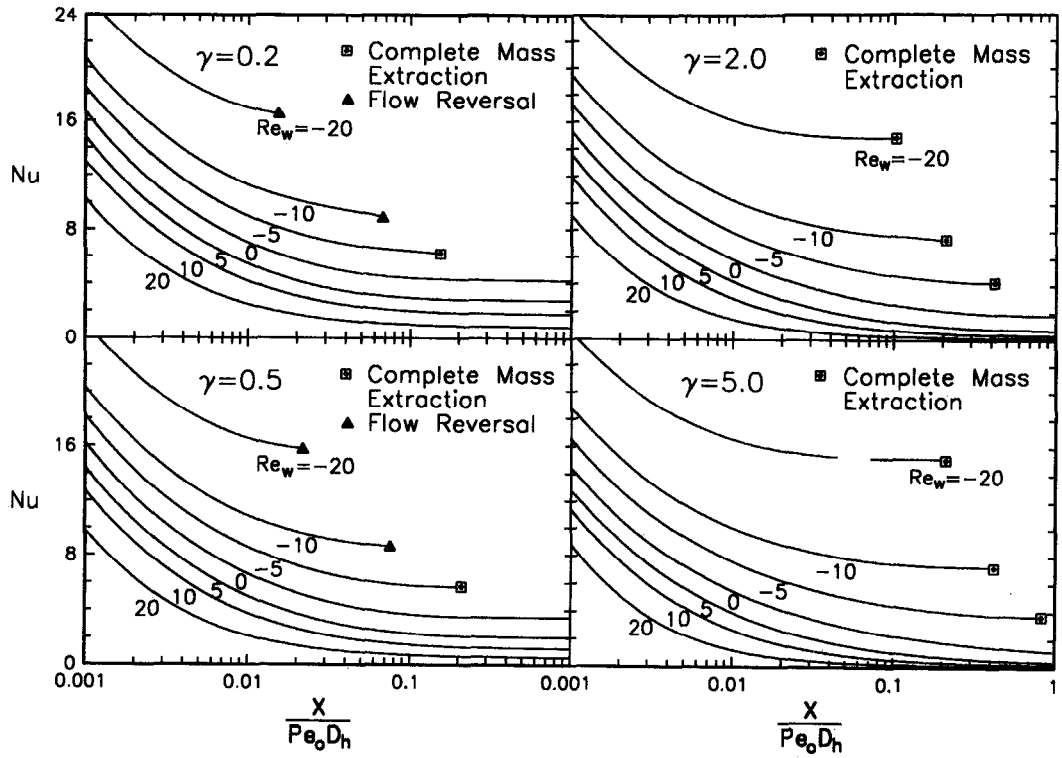

FIG. 10. Variations of Nusselt numbers along the axial direction for $Pr = 0.72$, $\gamma = 0.2$, 0.5, 2.0 and 5.0 with various values of Re_w.

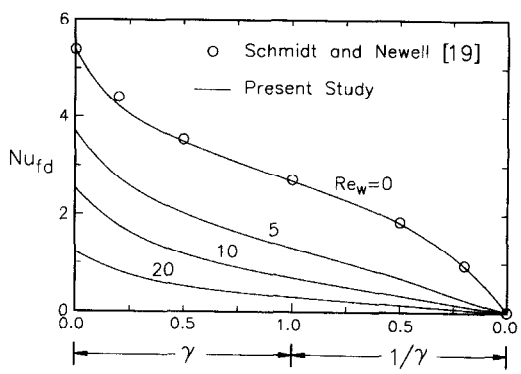

FIG. 11. Fully developed Nusselt numbers of various injection flows in the rectangular ducts.

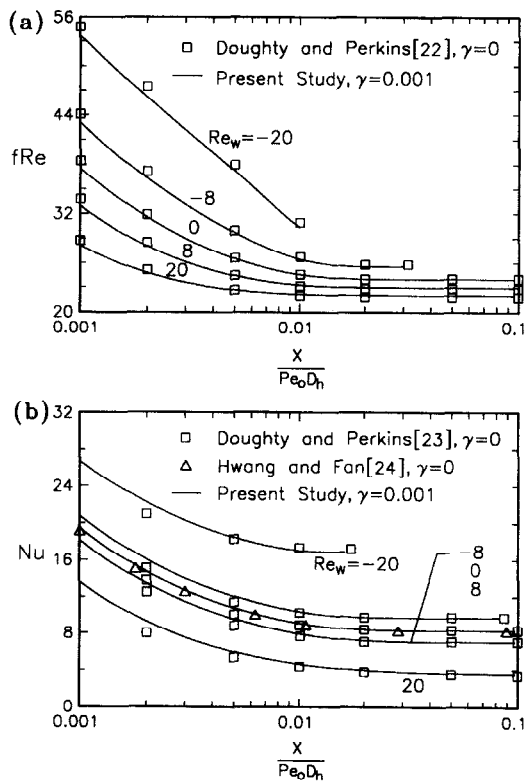

FIG. 12. Comparison of calculated results with the existing data for (a) fRe, (b) Nu.

in Fig. 12(b) for comparison with the existing data [23]. The present results fit Doughty and Perkins' data very well except those near the inlet region. However, the present results for $Re_w = 0$ also fit Hwang and Fan's data [24] well along the entire axial axis.

CONCLUSIONS

(1) The axial pressure drop in a rectangular duct is increased for the injection flow and decreased for the suction flow as compared with the impermeable flow. However, the pressure recovery appears downstream

for suction flow with small aspect ratio due to flow reversal, and a change to turbulent flow may be expected.

(2) It is shown that fluid injection increases the friction factor and reduces the hydrodynamic entrance length. However, a fully developed region cannot always be achieved in suction flow due to mass extraction and flow reversal.

(3) It has been verified that the wall heat transfer decreases in injection flow and increases in suction flow. Also, the thermal entrance length is increased with the fluid injection.

(4) For the effect of aspect ratio, Nusselt number is decreased with the increase in the aspect ratio due to larger thermal resistance through the cross section, and the flow finds it difficult to reach its thermally fully developed region in the same situation.

Acknowledgements—This study is supported by the Energy Commission of the Ministry of Economic Affairs of Taiwan, Republic of China through Fuel Cell Project No. 38K2100. The authors also acknowledge the assistance of the Energy and Resources Laboratories, ITRI for the use of a computer.

REFERENCES

1. W. M. Massey, Jr., Heat and mass transfer in semiporous channels, PhD Thesis, Georgia Institute of Technology, Atlanta, Georgia (1969).
2. S. J. Rhee and D. K. Edwards, Laminar entrance flow in a flat plate duct with asymmetric suction and heating, *Numer. Heat Transfer* **4,** 85–100 (1981).
3. M. M. Sorour and M. A. Hassab, Effect of sucking the hot fluid film on the performance of flat plate solar energy collectors, *Appl. Energy* **14,** 161–173 (1983).
4. J. Jorne, Mass transfer in laminar flow channel with porous wall, *J. Electrochem. Soc.* **129,** 1727–1733 (1982).
5. P. Lessner and J. Newman, Hydrodynamics and mass transfer in a porous-wall channel, *J. Electrochem. Soc.* **131,** 1828–1831 (1984).
6. C. Y. Soong and G. J. Hwang, Laminar mixed convection in a radially rotating semiporous channel, *Int. J. Heat Mass Transfer* **33,** 1805–1816 (1990).
7. G. J. Hwang, Y. C. Cheng and M. L. Ng, Friction factors and heat transfer in a square duct with one-walled injection and suction, *Int. J. Heat Mass Transfer* **36,** 2429–2440 (1993).
8. G. J. Hwang, Y. C. Cheng and M. L. Ng, Friction factor and heat transfer correlations for gaseous reactant flow in fuel cell power modules, *Proceedings of 6th International Symposium on Transport Phenomena in Thermal Engineering*, Vol. 1, pp. 685–690 (1993).
9. K. A. Alkasab and C. Y. Lu, Transient effects of changing the electric load on the performance of phosphoric acid fuel cell power plant, *Int. J. Energy Systems* **3,** 9–17 (1985).
10. N. E. Vanderbough, J. R. Huff and J. Hedstrom, Heat and mass transfer in PEM fuel cells, *Proceedings of 24th IECEC*, Vol. 3, pp. 1637–1640 (1989).
11. T. Okada, H. Ide, M. Tanaka, S. Narita and J. Ohtsuki, Study of temperature control in indirect internal reforming MCFC stack, *Proceedings of 25th IECEC*, Vol. 3, pp. 207–212 (1990).
12. P. L. Donoughe, Analysis of laminar incompressible flow in semiporous channels, TN-3759, NACA (1956).
13. E. R. G. Eckert, P. L. Donoughe and B. J. Moore, Velocity and friction characteristics of laminar viscous boundary-layer and channel flow over surfaces with ejection and suction, TN-4102, NACA (1957).
14. F. M. White, Laminar flow in porous ducts, PhD Thesis, Georgia Institute of Technology, Atlanta, Georgia (1959).
15. M. M. Sorour, M. A. Hassab and S. Estafanous, Developing laminar flow in a semiporous two-dimensional channel with nonuniform transpiration, *Int. J. Heat Fluid Flow* **10,** 44–54 (1987).
16. F. C. Chou and G. J. Hwang, Vorticity–velocity method for the Graetz problem and the effect of natural convection in a horizontal rectangular channel with uniform wall heat flux, *J. Heat Transfer* **109,** 704–710 (1987).
17. R. M. Curr, D. Sharma and D. G. Tanchell, Numerical prediction of some three-dimensional boundary layers in ducts, *Comput. Meth. Appl. Mech. Engng* **1,** 143–158 (1972).
18. R. A. Shah and A. L. London, *Laminar Flow Forced Convection in Ducts*, Suppl. 1 *to Advanced Heat Transfer*, pp. 196–222, Academic Press, New York (1978).
19. F. M. Schmidt and M. E. Newell, Heat transfer in fully developed laminar flow through rectangular and isosceles triangular ducts, *Int. J. Heat Mass Transfer* **10,** 1121–1128 (1967).
20. J. P. Quaile and E. K. Levy, Laminar flow in a porous tube with suction, *J. Heat Transfer* **97,** 66–71 (1975).
21. R. J. Pederson and R. B. Kinney, Entrance-region heat transfer for laminar flow in porous tubes, *Int. J. Heat Mass Transfer* **14,** 159–161 (1971).
22. J. R. Doughty and H. C. Perkins, Jr., Hydrodynamic entry problems for laminar flow between parallel porous plates, *J. Appl. Mech.* **92,** 548–550 (1970).
23. J. R. Doughty and H. C. Perkins, Jr., Thermal and combined entry problems for laminar flow between parallel porous plates, *J. Heat Transfer* **94,** 233–234 (1972).
24. C. L. Hwang and L. T. Fan, Finite difference analysis of forced convection heat transfer in entrance region of a flat rectangular duct, *Appl. Sci. Res.* **13A,** 401–422 (1964).